Title

Quantitative analysis of unruptured intracranial aneurysm wall thickness and enhancement using 7T high resolution, black blood magnetic resonance imaging

Journal

Journal of NeuroInterventional Surgery, 14(7)

ISSN

1759-8478

Authors

Liu, Xinke
Feng, Junqiang
Li, Zhixin
et al.

Publication Date

2022-07-01

DOI

10.1136/neurintsurg-2021-017688

Peer reviewed

HHS Public Access

Author manuscript

J Neurointerv Surg. Author manuscript; available in PMC 2022 September 01.

Published in final edited form as:

J Neurointerv Surg. 2022 July ; 14(7): 723–728. doi:10.1136/neurintsurg-2021-017688.

Quantitative analysis of unruptured intracranial aneurysm wall thickness and enhancement using 7T high resolution, black blood magnetic resonance imaging

Xinke Liu[1], **Junqiang Feng**[1], **Zhixin Li**[2,3], **Zihao Zhang**[2,3], **Qiang Zhang**[4], **Yuhua Jiang**[1], **Xiaochuan Huo**[1], **Xubin Chai**[2,3], **Yue Wu**[2,3], **Qingle Kong**[5], **Peng Liu**[1], **Huijian Ge**[1], **Hengwei Jin**[1], **Jing An**[6], **Peng Jiang**[1], **David A Saloner**[7], **Youxiang Li**[1], **Chengcheng Zhu**[8]

[1]Department of Interventional Neuroradiology, Beijing Neurosurgical Institute and Beijing Tiantan Hospital, Capital Medical University, Beijing, China

[2]State Key Laboratory of Brain and Cognitive Science, Institute of Biophysics, Chinese Academy of Sciences, 15 Datun Road, Beijing 100101, China

[3]University of Chinese Academy of Sciences, Beijing 100049, China

[4]Center for Biomedical Imaging Research, Department of Biomedical Engineering, School of Medicine, Tsinghua University, Beijing, China

[5]MR Collaboration, Siemens Healthcare China, Beijing, China

[6]Siemens Shenzhen Magnetic Resonance Ltd, Siemens Healthcare China, Shenzhen, China

[7]Department of Radiology and Biomedical Imaging, University of California San Francisco, San Francisco, California, USA

[8]Department of Radiology, University of Washington, Seattle, Washington, USA

Abstract

Correspondence to Dr Zihao Zhang, State Key Laboratory of Brain and Cognitive Science, Institute of Biophysics, Chinese Academy of Sciences, 15 Datun Road, Beijing 100101, China; zhzhang@ibp.ac.cn and Professor Youxiang Li, Department of Interventional Neuroradiology, Beijing Neurosurgical Institute and Beijing Tiantan Hospital, Capital Medical University, Beijing 100070, China; liyouxiang@263.net.

XL and JF contributed equally.

XL and JF are joint first authors.

Contributors Protocol/project development: XL, ZZ, CZ, and YL. Data collection or management: JF, ZL, LP, XH, YJ, PJ, QK, XC, YW, HG, HJ, and JA. Data analysis: XL, JF, ZL, QZ, DAS, and CZ.

Competing interests None declared.

Patient consent for publication Not required.

Ethics approval This study was conducted under institutional review board approval at Beijing Tiantan Hospital (ID No KY2017-057-02).

Provenance and peer review Not commissioned; externally peer reviewed.

Data availability statement Data are available upon reasonable request.

Background—This study was performed to quantify intracranial aneurysm wall thickness (AWT) and enhancement using 7T MRI, and their relationship with aneurysm size and type.

Methods—27 patients with 29 intracranial aneurysms were included. Three-dimensional T1 weighted pre- and post-contrast fast spin echo with 0.4 mm isotropic resolution was used. AWT was defined as the full width at half maximum on profiles of signal intensity across the aneurysm wall on pre-contrast images. Enhancement ratio (ER) was defined as the signal intensity of the aneurysm wall over that of the brain parenchyma. The relationships between AWT, ER, and aneurysm size and type were investigated.

Results—7T MRI revealed large variations in AWT (range 0.11–1.24 mm). Large aneurysms (>7 mm) had thicker walls than small aneurysms (≤7 mm) (0.49±0.05 vs 0.41±0.05 mm, $p<0.001$). AWT was similar between saccular and fusiform aneurysms ($p=0.546$). Within each aneurysm, a thicker aneurysm wall was associated with increased enhancement in 28 of 29 aneurysms (average $r=0.65$, $p<0.05$). Thicker walls were observed in enhanced segments (ER >1) than in non-enhanced segments (0.53±0.09 vs 0.38±0.07 mm, $p<0.001$).

Conclusion—Improved image quality at 7T allowed quantification of intracranial AWT and enhancement. A thicker aneurysm wall was observed in larger aneurysms and was associated with stronger enhancement.

INTRODUCTION

Intracranial aneurysms reportedly occur in 3.2% (95% CI 1.9% to 5.2%) of the world population.[1] Intracranial aneurysms are characterized by low rupture rates,[2] high morbidity and mortality rates following rupture, and non-negligible treatment related complications.[3] Therefore, rupture risk stratification is an important topic in intracranial aneurysm research. Compared with traditional imaging approaches that only provide information on aneurysmal lumen morphology, recent advances in MRI enable us to directly visualize the aneurysm wall. Aneurysm wall enhancement (AWE) has been noted following the administration of gadolinium based contrast agents, and AWE has been studied as a potential indicator of aneurysm instability.[4–6] However, the underlying mechanism and clinical relevance of AWE remain controversial.[7 8] Aneurysm wall thickness (AWT) has also been studied as a potential risk factor for aneurysm rupture, and previous histological studies have shown that AWT varies within the aneurysm and differs between ruptured and unruptured aneurysms.[9–11] Some studies have shown that aneurysm rupture can occur at locations of wall thinning, whereas other studies have shown that a thickened wall is associated with atherosclerosis. However, studying AWT in vivo is challenging,[12 13] mostly because of insufficient spatial resolution, and hence 7T MRI, which allows higher resolution and better image quality, may improve the ability to quantify AWT. The link between AWE and AWT is also poorly understood. A recent histological study revealed that a thickened aneurysm wall accompanied by inflammatory cell infiltration and vasa vasorum development might be correlated with AWE.[14]

This study was performed to (i) quantify intracranial AWT and AWE using 7T high resolution black blood MRI (0.4 mm isotropic resolution) and histologically validate AWT measurements when available and (ii) study the relationship between the AWT and AWE

and investigate the associations of AWT with aneurysm size and type. We hypothesized that 7T MRI can differentiate the thick and thin regions of the aneurysm wall with reasonable accuracy to quantify AWT, and that AWT and AWE are correlated with each other and with aneurysm size and type.

MATERIALS AND METHODS

Patients

Patients with unruptured intracranial aneurysms were recruited through our endovascular treatment clinic from November 2015 to July 2017. Inclusion criteria were age 18–80 years, diagnosis of an intracranial aneurysm, and ability to cooperate during the MRI examination. Patients with contraindications to 7.0 T MRI (including claustrophobia, metal objects such as prostheses in or on the body, or clips or coils used for previous aneurysm treatment) were excluded, as were patients with arterial dissection. The study was approved by the institutional review board, and informed consent was obtained from each patient.

Imaging protocol

Images were acquired on a 7T MRI research system (Siemens Medical Systems, Erlangen, Germany) equipped with a Nova 32 channel head coil. Patients were asked to lie on a supporting device that helped them maintain the same head position throughout the scan. The sequences used were three-dimensional (3D) time-of-flight magnetic resonance angiography (TOF-MRA) and pre- and post-contrast black blood SPACE (fast spin echo with variable flip angle trains).[15] Three-dimensional TOF-MRA was used to locate the aneurysm and assess the geometry with a repetition time of 18 ms, echo time of 4.96 ms, flip angle of 24°, field of view of 210×164 mm^2, voxel size of 0.33×0.33 × 0.40 mm^3, six slabs, and acquisition time of 9.16 min. This was followed by an optimized prototype pre-contrast SPACE sequence that was used to acquire black blood images.[4 15] The following parameters were used in SPACE at 7T: repetition time of 1200 ms, echo time of 16 ms, field of view of 181×181 mm^2, GRAPPA of 3, voxel size of 0.40×0.40 × 0.40 mm^3, echo train length of 50, and acquisition time of 10.29 min. A low flip angle train design was used to achieve narrower point spread function and improved sharpness, as adopted from a previous publication.[15] After the pre-contrast SPACE sequence acquisition, a gadolinium based contrast agent (GE Healthcare, Chicago, Illinois, USA) was injected through the antecubital vein as a bolus at 5 mL/s and a dose of 0.1 mmol/kg of body weight; this was immediately followed by a 10 mL saline flush. A post-contrast SPACE scan was performed 15 min after contrast injection. Total study time was approximately 30 min.

Image post-processing

All image post-processing was performed using a graphical user interface program developed using MATLAB (MathWorks, Natick, Massachusetts, USA). Image data were reformatted in planes parallel to the inlet vessels. The pre- and post-contrast images were co-registered by two neuroradiologists based on the image features. Three consecutive axial, sagittal, and coronal slices (total of nine slices for each aneurysm), through the region of the aneurysm with the largest cross sectional area and where >75% of the outer wall boundary could be differentiated from the brain parenchyma, were selected. The outer

contour of the aneurysm was manually drawn on both the pre- and post-contrast images by two neuroradiologists. Radial lines were then automatically generated from the center of the aneurysm to the outer wall, and 16 circumferential segments were defined. The dimensions of each segment were thus comparable with the size of a single voxel. Profiles of signal intensity were determined across the aneurysm wall for each radial line. Measurements were independently completed by two experienced radiologists to study the reproducibility of the methodology.

On pre-contrast images, the location of half peak intensity was determined on both the inner and outer walls of the aneurysm, and AWT was defined as the full width at half maximum point (figure 1).[15] Specific segment measurement data were dropped off when the outer wall of the aneurysm could not be differentiated from the adjacent brain tissue.

On post-contrast images, the enhancement ratio (ER) was determined by first identifying SI_{wall}, defined as the maximum signal intensity along the radial lines and within the outer wall on the post-contrast images. This was then compared with SI_{brain}, defined as the mean signal intensity in a 10 pixel diameter circle of nearby brain parenchyma (white matter). Two experienced radiology reviewers (with 10 and 20 years of experience in neuroradiology and neurovascular image analysis, respectively, and co-authors of this manuscript) confirmed the selection of the reference structure. Online supplemental figure 1 shows the location and region of interest drawn on the white matter to calculate SI_{brain} in two cases. The surrounding adjacent white matter had relatively homogenous signal intensities, and locations with small vessels or white matter abnormalities were avoided (such as infarctions or white matter hyperintensities) (online supplemental figure 1). ER was then defined as SI_{wall}/SI_{brain} on post-contrast images.[16–18] Segments with an ER value of >1 were regarded as enhancing, and those with an ER value of ≤1 were regarded as non-enhancing.

Aneurysm type classification and maximal diameter measurement were performed by two neuroradiologists, as previously described.[4] Intracranial aneurysms were further divided into a fusiform group and a saccular group according to shape, and into a >7 mm group and ≤7 mm group according to size.

Histological analysis

Aneurysm wall specimens were collected at surgery (clipping) for histological study when available. Routine histological analysis was performed. Formalin fixed and paraffin embedded specimens were cut into 2.5 μm thick tissue sections. Slides were stained with hematoxylin–eosin. Immunohistochemical staining was performed. The following primary antibodies were used: CD68 (M0814; Dako, Glostrup, Denmark) as an inflammatory marker and CD31 (M0823; Dako) to assess neoangiogenesis.

Statistics

All statistical analyses were performed with MATLAB 2017a (MathWorks). Pearson’s coefficient was adopted to detect the correlation between AWT and ER in each aneurysm and in the pooled dataset of 32 aneurysms. The t test was performed to detect the difference between segments with an ER of ≤1 and those with an ER of >1 in a single aneurysm

and in the pooled dataset. The Q value was calculated using multiple testing correction (Benjamini–Hochberg method) to correct the p value of these multiple comparisons (multiple slices in one aneurysm). AWT in the saccular and fusiform groups and in the >7 mm and ≤7 mm groups were compared using the t test. A p value or Q value of 0.05 was used as the threshold of statistical significance.

RESULTS

Thirty-four patients underwent both pre- and post-contrast vessel wall imaging (VWI) by 7T MRI. The following patients and aneurysms were excluded: three patients with cavernous sinus aneurysms that had significant signal loss due to 7T MRI susceptibility artifacts, one patient with small aneurysms (<5 mm and difficult to define in three contiguous slices), and three aneurysms with severe intraluminal noise. In total, 27 patients (mean age 50±17 years) with 29 intracranial aneurysms (11 fusiform and 18 saccular) were included. Baseline data for the patients, and AWT and ER measurement results are presented in table 1. Agreement between the two observers who drew the out-contour was excellent, with an intraclass correlation coefficient (ICC) of 0.941 (95% CI 0.936 to 0.946) for the AWT measurement and 0.942 (95% CI 0.936 to 0.946) for the ER measurement (online supplemental figure 2B, C).

Quantification of AWT

Measured AWT for each aneurysm is shown in table 1. We found that 7T MRI provided good image quality in differentiating thick and thin regions of the vessel wall within an aneurysm and among different aneurysms. AWT ranged widely from 0.11 to 1.24 mm. Within each aneurysm, the maximal AWT was 3.6 times the minimal AWT (0.90±0.18 vs 0.25±0.09 mm, $p<0.01$). AWT in the >7 mm group (0.49±0.05 mm) was significantly larger than that in the ≤7 mm group (0.41±0.05 mm) ($p<0.001$). AWT was not significantly different between the fusiform group (0.45±0.07 mm) and saccular group (0.44±0.06 mm) ($p=0.546$).

Correlation of AWT and AWE

The correlation of AWT and ER for every individual aneurysm is presented in table 1. Almost all aneurysms (28 of 29) showed a significant positive correlation between AWT and ER, with average r value of 0.65 (range 0.25–0.87) ($p<0.05$) (figure 2). After pooling all segments from all patients, the r value was 0.51 ($p<0.001$) (online supplemental figure 2A). One aneurysm showed no significant correlation between AWT and ER, and one aneurysm had no segments with an ER of >1.

For all aneurysms, average AWT for the ER ≤1 and ER >1 groups are listed in table 1. Of 28 aneurysms, 25 showed a significant difference in AWT between sections with an ER of ≤1 and >1. Three aneurysms showed no significant difference because few segments had an ER of ≤1. A pooled analysis of 28 aneurysms showed that the mean AWT of segments with an ER of >1 was significantly larger than that of segments with an ER of ≤1 (0.53±0.09 vs 0.38±0.07 mm, $p<0.001$).

Histological analysis

One aneurysm specimen was harvested from an adult patient with a 7 mm anterior communicating artery aneurysm for histological analysis (figure 3). The specimen was collected 1 week after the MRI scan. MRI showed focal AWE at the thick part of the vessel wall and a variable AWT (0.33–0.87 mm). Histological analysis showed that AWT was heterogeneous, and the thickness ranged from 0.22 to 0.84 mm, which was comparable with the measurement from the in vivo 7T MRI examination. Immunohistochemistry demonstrated that an abundant vasa vasorum had developed at the tunica adventitia at the thickened site; little inflammatory cell infiltration was observed.

DISCUSSION

In this study, we used 7T MRI, with 0.4 mm isotropic high resolution, to quantify AWT and AWE, and found that 7T MRI differentiated variable AWT values; a thicker wall was correlated with higher enhancement, and larger aneurysms had thicker walls than smaller aneurysms. Furthermore, our histological analysis showed that AWT had good agreement with the 7T MRI findings, indicating that 7T MRI has the potential to accurately quantify AWT. The histological analysis also showed that the vasa vasorum developed in the thickened part, which appeared as AWE in 7T MRI.

Aneurysm wall composition or thickness might provide critical information regarding aneurysm development or rupture, but little investigation of AWT has been performed because of the difficulty in imaging. Sherif *et al*[12] attempted to measure AWT on experimental aneurysms. Their manual measurement showed unacceptable inaccuracies because AWT was below the image resolution threshold. In another study, Blankena *et al*[13] used 7T MRI with an isotropic resolution of 0.8 mm to measure AWT. They used the normalized maximal signal intensity on the aneurysm wall to depict AWT and found that in vivo imaging of AWT variation was possible on 7T MRI. However, the maximal intensity that they used to measure AWT might have been severely impacted by image noise, motion artifacts, and field inhomogeneity at 7T. In our study, the signal intensity profile of every point on the aneurysm wall was plotted. To reduce the partial volume effect and nearby noise interference, AWT was defined as the distance between the two points when the signal intensity of the inner and outer walls reached half of the peak value. The current resolution (0.4 mm) is the highest resolution used in research to date. However, it is still insufficient for accurate measurement of thickness because the scale of AWT and voxel size are very close and because spatial blurring is inherent to SPACE because of the use of a long echo train.[15] Despite this, the variation in AWT for different aneurysms showed good agreement with what we observed. Finally, we used an automatic thickness measurement method in this study.

There are different assumptions about the mechanism of AWE,[19–21] and different hypotheses might lead to different interpretations of the clinical significance, such as an unstable state or higher rupture risk.[4 7 22 23] Samaniego *et al*[24] recently analyzed enhancement of the aneurysm wall and its parent artery and found that an inflammatory process in the wall of the parent artery may lead to aneurysm formation and growth. In the present study, we found that stronger AWE corresponded to a greater AWT. However, our

result is inconsistent with that of a previous study showing that wall thickening accompanied by atherosclerosis and neovascularization corresponded to visualization of AWE.[25] Limited knowledge is available regarding whether the thinner or thicker portion of the wall is a potential rupture site.[10] Therefore, we are inclined to conclude that AWE more likely represents the active remodeling process of the aneurysm wall than a higher rupture risk.

We also found that the mean AWT in large aneurysms (>7 mm) was significantly greater than that in small aneurysms (≤7 mm). Our results are similar to those of another study showing that smaller aneurysms (<7 mm) had a higher proportion of super thin tissue and a lower thick tissue content.[11] Because a thickened wall is usually accompanied by atherosclerotic change and neovascularization, this size–thickness relationship might indicate the advanced stage of the aneurysm remodeling process. A difference in the AWT was also observed between fusiform and saccular aneurysms. However, the difference did not reach statistical significance, possibly because of the small sample size.

Although AWE has been widely reported, most enhancement analyses were based on subjective assessment.[5 22 26 27] Several studies have been performed in an attempt to quantify the aneurysm wall ER.[4 17 28] To evaluate AWE, previous studies have used different reference structures that either enhance or do not enhance after contrast injection. Unfortunately, a standard for which reference structure to use is still lacking. However, the adjacent white matter (which does not enhance)[16–18] and the low infundibulum (which does enhance)[29] are the two most commonly used reference structures in previous publications. At 7T, because of the inhomogeneous B0 field at the skull base, signal loss or imaging artifacts near the infundibulum are commonly observed.[30] Therefore, we used the adjacent white matter as the reference structure. Using the adjacent white matter as a reference has good inter-reader reproducibility, as shown in previous studies (ICC values of 0.98, 0.92, 0.74, and 0.975).[16–18] In our study, measurement of ER was also highly reproducible (inter-reader ICC=0.942). In addition, the Bland–Altman plots in this study showed good agreement between the two readers.

Several studies have used histology to explore AWE mechanisms.[9 26] Shimonaga *et al*[14] performed both VWI and histological analysis on nine patients with unruptured aneurysms. They found that wall thickening accompanied by neovascularization and macrophage infiltration corresponded to AWE. In our study, one aneurysm specimen was harvested from a partially enhancing aneurysm. We observed similar degenerative changes in the histological analysis. Because it is difficult to strictly match the specimen with the VWI findings, quantitative measurement and correlation analysis of AWT and ER with VWI data provide an improved understanding of the pathophysiological changes in the aneurysm wall. Whether the aneurysm wall is enhanced through the vasa vasorum pathway requires further exploration.

Our study has several limitations. First, although the resolution of 7T VWI has been improved over 3T, it is still challenging to accurately characterize AWT; however, we proved that 7T imaging can differentiate between thick and thin regions of the aneurysm wall. Second, the ER calculation was performed only with reference to the post-contrast image. Because the aneurysm wall is very thin, a small registration error can lead to a

large calculation error. Third, we were able to harvest a surgical specimen for histological validation in only one aneurysm, and it proved difficult on histology to accurately match the thickened regions to the enhanced regions, as determined on VWI. A larger scale histological validation study would be valuable to confirm the findings in this study. This in vivo evaluation of AWT and AWE using ultra high resolution 7T MRI (0.4 mm isotropic, the highest resolution in the literature to date) may enrich our understanding of the pathology of intracranial aneurysms. Fourth, we only performed analysis in nine slices in three planes of the aneurysm (three axial, three sagittal, and three coronal slices, covering about 30–50% of the entire wall depending on aneurysm size). Most previous studies of intracranial AWE used similar approaches (selecting 1–3 slices)[16–18 29] and showed good inter-reader reproducibility; our own data also showed good inter-reader reproducibility. A true 3D analysis of AWT and AWE is the best option. However, developing a tool to reconstruct the 3D geometry and using the full width at half maximum method to quantify AWT and AWE is not easy; it requires extensive work for algorithm development and validation. To the best of our knowledge, only one paper has three-dimensionally quantified the intracranial AWT (but only partially),[13] and no study has yet performed a 3D quantification of AWE. A 3D analysis would provide richer information to understand the location specific AWT and AWE. A future study using 3D analysis is needed to confirm our findings. All of these factors may limit the conclusions of these studies.

CONCLUSIONS

Improved image quality at 7T allowed for quantification of intracranial AWT and AWE in vivo. Thicker aneurysm walls were observed in larger aneurysms and were associated with stronger enhancement. These imaging findings need to be further validated in larger scale histological studies.

Supplementary Material

Refer to Web version on PubMed Central for supplementary material.

Funding

This work was supported by the National Natural Science Foundation of China (82001804, 81901197 and 31730039); the Natural Science Foundation of Beijing Municipality (7191003); the Ministry of Science and Technology of China (2019YFA0707103); and the Chinese Academy of Sciences (XDB32010300). Chengcheng Zhu is supported by the US National Institutes of Health (NIH) grant R00HL136883.

REFERENCES

1. Go AS, Mozaffarian D, Roger VL, et al. Heart disease and stroke statistics--2014 update: a report from the American Heart Association. Circulation 2014;129:e28–92. [PubMed: 24352519]
2. UCAS Japan Investigators, Morita A, Kirino T, et al. The natural course of unruptured cerebral aneurysms in a Japanese cohort. N Engl J Med 2012;366:2474–82. [PubMed: 22738097]
3. Wiebers DO, Whisnant JP, Huston J, et al. Unruptured intracranial aneurysms: natural history, clinical outcome, and risks of surgical and endovascular treatment. Lancet 2003;362:103–10. [PubMed: 12867109]

4. Liu X, Zhang Z, Zhu C, et al. Wall enhancement of intracranial saccular and fusiform aneurysms may differ in intensity and extension: a pilot study using 7-T high-resolution black-blood MRI. Eur Radiol 2020;30:301–7. [PubMed: 31218429]
5. Edjlali M, Guédon A, Ben Hassen W, Boulouis G, et al. Circumferential thick enhancement at vessel wall MRI has high specificity for intracranial aneurysm instability. Radiology 2018;289:181–7. [PubMed: 29969070]
6. Matsushige T, Shimonaga K, Ishii D, et al. Vessel wall imaging of evolving unruptured intracranial aneurysms. Stroke 2019;50:1891–4. [PubMed: 31167619]
7. Larsen N, von der Brelie C, Trick D, et al. Vessel wall enhancement in unruptured intracranial aneurysms: an indicator for higher risk of rupture? High-resolution MR imaging and correlated histologic findings. AJNR Am J Neuroradiol 2018;39:1617–21 [PubMed: 30026386]
8. Nguyen VL, Backes WH, Kooi ME, et al. Quantification of abdominal aortic aneurysm wall enhancement with dynamic contrast-enhanced MRI: feasibility, reproducibility, and initial experience. J Magn Reson Imaging 2014;39:1449–56. [PubMed: 24151142]
9. Frösen J, Piippo A, Paetau A, et al. Remodeling of saccular cerebral artery aneurysm wall is associated with rupture: histological analysis of 24 unruptured and 42 ruptured cases. Stroke 2004;35:2287–93. [PubMed: 15322297]
10. Morel S, Diagbouga MR, Dupuy N, et al. Correlating clinical risk factors and histological features in ruptured and unruptured human intracranial aneurysms: the Swiss AneuX study. J Neuropathol Exp Neurol 2018;77:555–66. [PubMed: 29688417]
11. Kadasi LM, Dent WC, Malek AM. Cerebral aneurysm wall thickness analysis using intraoperative microscopy: effect of size and gender on thin translucent regions. J Neurointerv Surg 2013;5:201–6. [PubMed: 22387724]
12. Sherif C, Kleinpeter G, Loyoddin M, et al. Aneurysm wall thickness measurements of experimental aneurysms: in vivo high-field MR imaging versus direct microscopy. Acta Neurochir Suppl 2015;120:17–20. [PubMed: 25366593]
13. Blankena R, Kleinloog R, Verweij BH, et al. Thinner regions of intracranial aneurysm wall correlate with regions of higher wall shear stress: a 7T MRI study. AJNR Am J Neuroradiol 2016;37:1310–7. [PubMed: 26892986]
14. Shimonaga K, Matsushige T, Ishii D, et al. Clinicopathological insights from vessel wall imaging of unruptured intracranial aneurysms. Stroke 2018;49:2516–9. [PubMed: 30355091]
15. Zhu C, Haraldsson H, Tian B, et al. High resolution imaging of the intracranial vessel wall at 3 and 7 T using 3D fast spin echo MRI. Magn Reson Mater Phy 2016;29:559–70.
16. Fu Q, Wang Y, Zhang Y, et al. Qualitative and quantitative wall enhancement on magnetic resonance imaging is associated with symptoms of unruptured intracranial aneurysms. Stroke 2021;52:213–22. [PubMed: 33349014]
17. Omodaka S, Endo H, Niizuma K, et al. Quantitative assessment of circumferential enhancement along the wall of cerebral aneurysms using MR imaging. AJNR Am J Neuroradiol 2016;37:1262–6. [PubMed: 26939634]
18. Qi H, Liu X, Liu P, et al. Complementary roles of dynamic contrast-enhanced MR imaging and postcontrast vessel wall imaging in detecting high-risk intracranial aneurysms. AJNR Am J Neuroradiol 2019;40:490–6. [PubMed: 30792252]
19. Hasan DM, Mahaney KB, Magnotta VA, et al. Macrophage imaging within human cerebral aneurysms wall using ferumoxytol-enhanced MRI: a pilot study. Arterioscler Thromb Vasc Biol 2012;32:1032–8. [PubMed: 22328774]
20. Vakil P, Ansari SA, Cantrell CG, et al. Quantifying intracranial aneurysm wall permeability for risk assessment using dynamic contrast-enhanced MRI: a pilot study. AJNR Am J Neuroradiol 2015;36:953–9. [PubMed: 25655875]
21. Kalsoum E, Chabernaud Negrier A, Tuilier T, et al. Blood flow mimicking aneurysmal wall enhancement: a diagnostic pitfall of vessel wall MRI using the postcontrast 3D turbo spin-echo MR imaging sequence. AJNR Am J Neuroradiol 2018;39:1065–7. [PubMed: 29599170]
22. Zhu C, Wang X, Degnan AJ, et al. Wall enhancement of intracranial unruptured aneurysm is associated with increased rupture risk and traditional risk factors. Eur Radiol 2018;28:5019–26. [PubMed: 29872913]

23. Samaniego EA, Roa JA, Hasan D. Vessel wall imaging in intracranial aneurysms. J Neurointerv Surg 2019;11:1105–12. [PubMed: 31337731]

24. Samaniego EA, Roa JA, Zhang H, et al. Increased contrast enhancement of the parent vessel of unruptured intracranial aneurysms in 7T MR imaging. J Neurointerv Surg 2020;12:1018–22. [PubMed: 32424006]

25. Nakatomi H, Segawa H, Kurata A, et al. Clinicopathological study of intracranial fusiform and dolichoectatic aneurysms: insight on the mechanism of growth. Stroke 2000;31:896–900. [PubMed: 10753995]

26. Hu P, Yang Q, Wang D-D, et al. Wall enhancement on high-resolution magnetic resonance imaging may predict an unsteady state of an intracranial saccular aneurysm. Neuroradiology 2016;58:979–85. [PubMed: 27438805]

27. Omodaka S, Endo H, Niizuma K, et al. Circumferential wall enhancement on magnetic resonance imaging is useful to identify rupture site in patients with multiple cerebral aneurysms. Neurosurgery 2018;82:638–44. [PubMed: 28586440]

28. Alexander MD, de Havenon A, Kim S-E, et al. Assessment of quantitative methods for enhancement measurement on vessel wall magnetic resonance imaging evaluation of intracranial atherosclerosis. Neuroradiology 2019;61:643–50. [PubMed: 30675639]

29. Omodaka S, Endo H, Niizuma K, et al. Circumferential wall enhancement in evolving intracranial aneurysms on magnetic resonance vessel wall imaging. J Neurosurg 2018:1–7.

30. Thomas BP, Welch EB, Niederhauser BD, et al. High-resolution 7T MRI of the human hippocampus in vivo. J Magn Reson Imaging 2008;28:1266–72. [PubMed: 18972336]

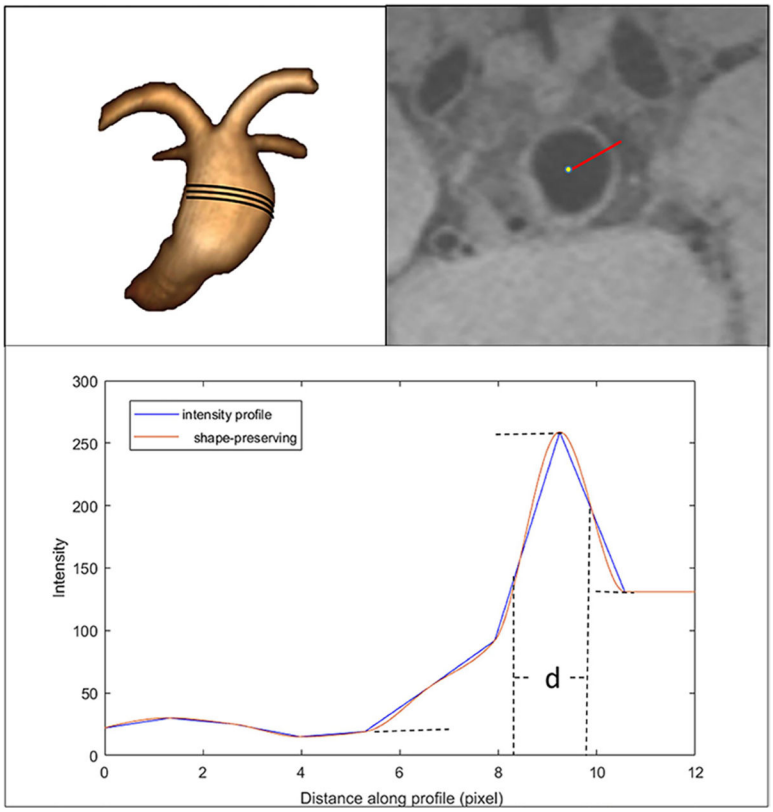

Figure 1.

Algorithm of aneurysm wall thickness calculation. Top left: fusiform basilar aneurysm. Top right: a line is drawn from the center of the aneurysm to the outside wall on a pre-contrast image. Bottom: signal intensity profile. The distance between two half peak points d×0.4 mm was defined as the thickness at that point.

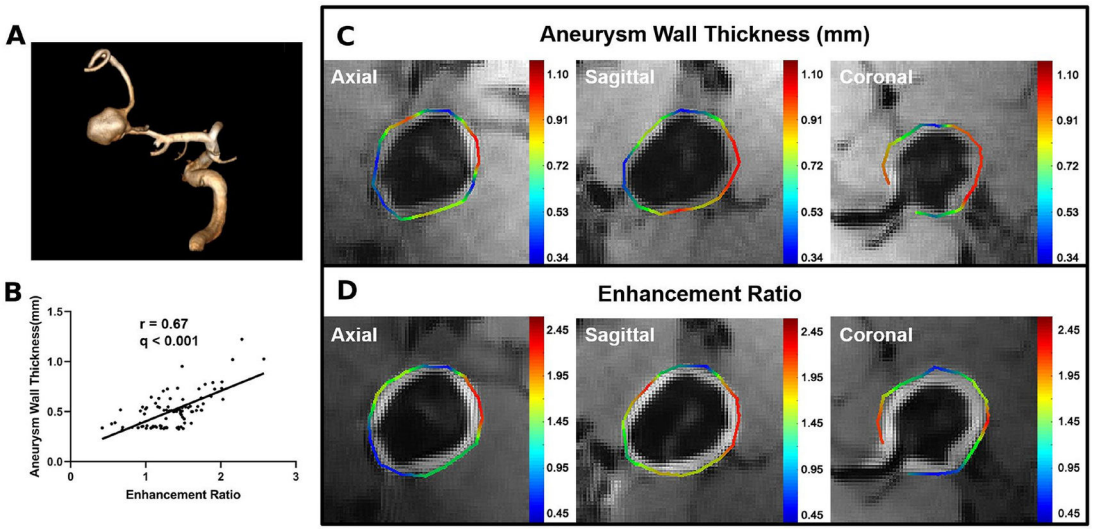

Figure 2.

Examples of the correlation between aneurysm wall thickness (AWT) and enhancement ratio (ER). (A) Volume rendering of time-of-flight magnetic resonance angiography of a middle cerebral artery aneurysm. (B) Pearson correlation plot shows a strong positive correlation between AWT and ER. (C) Colorful manually drawn out contour shows the calculation results of AWT on a pre-contrast image (color bar in mm). (D) Colorful manually drawn out contour shows the calculation results of the aneurysm wall ER on a post-contrast image.

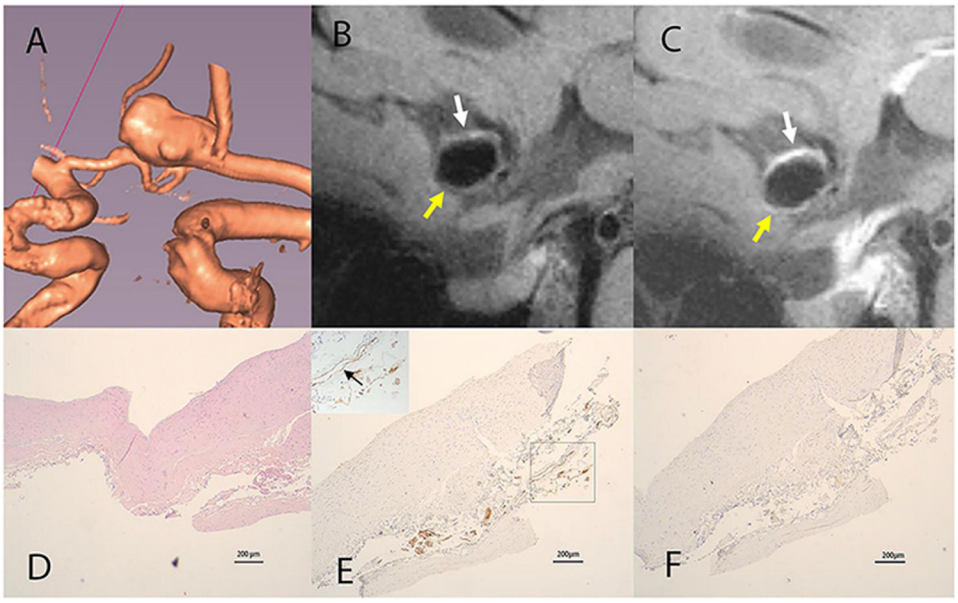

Figure 3.

(A) Volume rendering of an anterior communicating artery aneurysm. (B) Sagittal view of pre-contrast vessel wall imaging (VWI) shows a heterogeneous AWT (0.33–0.87 mm). The white arrow indicates the thickened part and the yellow arrow indicates the thinner parts. (C) Sagittal view of post-contrast VWI shows the thickened parts with greater enhancement (white arrow) and thinner parts with weak enhancement (yellow arrow). (D) Hematoxylin–eosin staining of the aneurysm wall shows a heterogeneous aneurysm wall (0.22–0.84 mm). (E) Immunohistochemical staining for CD31 shows development of an abundant vasa vasorum in the tunica adventitia (black arrow). (F) immunohistochemical staining for CD68 shows minimal macrophage cell infiltration. Scale bars indicate 200 μm for all histological images.

Table 1

Patient baseline data, and aneurysm wall thickness and enhancement ratio measurement results

Patient No	Location	Size (mm)	Category	R	P_R	Q_R	AWT_Enh (mm)	AWT_Non (mm)	P_T	Q_T	AWT range (mm)	ER range (mm)
1	ACoA	5	Saccular	0.86	<0.001*	<0.001*	0.43±0.13	0.26±0.03	<0.001*	<0.001*	(0.16–0.74)	(0.40–1.90)
2	R MCA	6.5	Saccular	0.87	<0.001*	<0.001*	0.65±0.10	0.37±0.11	<0.001*	<0.001*	(0.16–0.78)	(0.29–1.44)
3	L MCA	6.5	Saccular	0.84	<0.001*	<0.001*	0.74±0.14	0.45±0.13	<0.001*	<0.001*	(0.30–1.1 1)	(0.14–2.26)
4	R MCA	5	Saccular	0.81	<0.001*	<0.001*	0.54±0.14	0.31±0.11	<0.001*	<0.001*	(0.20–0.93)	(0.38–2.15)
5	ACoA	5.5	Saccular	0.76	<0.001*	<0.001*	0.42±0.13	0.29±0.05	<0.001*	<0.001*	(0.18–1.03)	(0.69–2.55)
6	BA	7	Saccular	0.63	<0.001*	<0.001*	0.61±0.10	0.42±0.07	<0.001*	<0.001*	(0.29–0.81)	(0.45–1.42)
7	L PCA	6.5	Saccular	0.74	<0.001*	<0.001*	0.55±0.12	0.34±0.10	<0.001*	<0.001*	(0.18–0.80)	(0.44–1.53)
8	L MCA	7	Saccular	0.79	<0.001*	<0.001*	0.62±0.15	0.36±0.12	<0.001*	<0.001*	(0.1 1–0.75)	(0.34–1.69)
9	ACA	5	Saccular	0.56	<0.001*	<0.001*	0.40±0.13	0.27±0.04	<0.001*	<0.001*	(0.23–0.82)	(0.71–2.31)
10	BA	6.5	Saccular	0.76	<0.001*	<0.001*	0.52±0.17	0.35±0.09	<0.001*	<0.001*	(0.21–1.00)	(0.14–2.40)
11	ACoA	10.5	Saccular	0.67	<0.001*	<0.001*	0.58±0.11	0.45±0.06	<0.001*	<0.001*	(0.33–0.87)	(0.35–1.65)
12	L MCA	5.1	Fusiform	0.56	<0.001*	<0.001*	0.41±0.12	0.30±0.07	<0.001*	<0.001*	(0.18–0.68)	(0.30–1.76)
13	ACoA	6	Saccular	0.60	<0.001*	<0.001*	0.43±0.13	0.32±0.08	<0.001*	<0.001*	(0.18–0.68)	(0.58–1.70)
14	L PCA	7.6	Fusiform	0.60	<0.001*	<0.001*	0.51±0.13	0.39±0.06	<0.001*	<0.001*	(0.26–0.97)	(0.39–1.64)
15	L MCA	5.9	Fusiform	0.82	<0.001*	<0.001*	0.52±0.25	0.32±0.09	<0.001*	<0.001*	(0.13–1.22)	(0.21–3.24)
16	R VA	8.1	Fusiform	0.66	<0.001*	<0.001*	0.60±0.08	0.41±0.08	<0.001*	<0.001*	(0.32–0.77)	(0.26–1.14)
17	BA	8.3	Fusiform	0.52	<0.001*	<0.001*	0.58±0.15	0.47±0.06	<0.001*	<0.001*	(0.41–1.17)	(0.33–2.34)
18	L MCA	6	Saccular	0.39	<0.001*	<0.001*	0.46±0.12	0.37±0.07	<0.001*	<0.001*	(0.24–0.85)	(0.38–2.13)
19	L VA	11.8	Fusiform	0.38	<0.001*	<0.001*	0.56±0.10	0.48±0.03	<0.001*	<0.001*	(0.44–0.76)	(0.77–2.56)
20	L MCA	8.4	Fusiform	0.87	<0.001*	<0.001*	0.54±0.17	0.39±0.06	<0.001*	<0.001*	(0.28–1.19)	(0.69–2.69)
21	L SCA	4.8	Fusiform	0.73	<0.001*	<0.001*	0.39±0.11	0.28±0.07	<0.001*	<0.001*	(0.16–0.57)	(0.71–1.52)
22	BA	8.3	Fusiform	0.70	<0.001*	<0.001*	0.60±0.16	0.40±0.08	0.001*	0.001*	(0.31–0.93)	(0.34–1.59)
23	L MCA	12	Saccular	0.77	<0.001*	<0.001*	0.66±0.24	0.44±0.11	0.001*	0.002*	(0.35–1.24)	(0.29–2.52)
24	ACoA	12	Saccular	0.61	0.001*	0.001*	0.57±0.15	0.46±0.06	0.011*	0.013*	(0.39–0.91)	(0.52–1.76)

J Neurointerv Surg. Author manuscript; available in PMC 2022 September 01.

Patient No	Location	Size (mm)	Category	R	P_R	Q_R	AWT_Enh (mm)	AWT_Non (mm)	P_T	Q_T	AWT range (mm)	ER range (mm)
25	L MCA	10	Saccular	0.67	<0.001*	<0.001*	0.53±0.18	0.41±0.08	0.011*	0.013*	(0.32–1.22)	(0.42–2.57)
26	R VA	5	Saccular	0.36	<0.001*	<0.001*	0.41±0.13	0.36±0.15	0.436	0.469	(0.18–0.86)	(0.20–2.16)
27	R ICA	12	Fusiform	0.25	0.056	0.056	0.48±0.10	0.47±0.09	0.771	0.800	(0.31–0.80)	(0.63–3.26)
28	R VA	7	Fusiform	0.37	<0.001*	<0.001*	0.44±0.10	0.44±0.10	0.971	0.971	(0.29–0.72)	(0.63–1.89)
29	ACoA	7.5	Saccular	0.69	<0.001*	<0.001*	NA	0.43±0.11	NA	NA	(0.18–0.80)	(0.11–1.00)

*p<0.05 or Q<0.05.

ACA, anterior cerebral artery; ACoA, anterior communicating artery; AWT, aneurysm wall thickness; BA, basilar artery; ER, enhancement ratio; ICA, internal carotid artery; L, left; MCA, middle cerebral artery; NA, not applicable; PCA, posterior cerebral artery; P_R, p value of correlation coefficient R; P_T, p value of t test; Q_R, corrected p value of correlation coefficient R using Benjamini-Hochberg procedure; Q_T, corrected p value of t test using Benjamini-Hochberg procedure; R, right; SCA, superior cerebellar artery; VA, vertebral artery.